Journal of Materials Science and Chemical Engineering, 2015, 3, 154-161
Published Online July 2015 in SciRes. http://www.scirp.org/journal/msce
http://dx.doi.org/10.4236/msce.2015.37021

The Preparation and Catalytic Performance of Nanoporous CuO/CeO_2 Composites

Caihua Wei, Xiaolong Zhang, Feifei Lu, Yanyan Song, Zhanbo Sun*

School of Science, Key Laboratory of Shaanxi for Advanced Functional Materials and Mesoscopic Physics, Key Laboratory for Non-Equilibrium Synthesis and Modulation of Condensed Matter, State Key Laboratory for Mechanical Behavior of Materials, Xi'an Jiaotong University, Xi'an, China
Email: *szb@mail.xjtu.edu.cn

Received 5 May 2015; accepted 9 July 2015; published 16 July 2015

Abstract

Nanoporous CuO/CeO_2 ribbons are successfully prepared through dealloying melt-spun $Al_{80-x}Cu_{20}Ce_x$ (x = 0.5, 1, 2, 3, at%) alloy in a 5 wt% NaOH aqueous solution, followed by calcining in air. The samples are characterized by XRD, SEM, EDS, HRTEM, Raman and gas chromatograph. For the dealloyed melt-spun $Al_{80-x}Cu_{20}Ce_x$ (x = 0.5, 1, 2, 3, at%) alloy, the XRD results indicate that Cu and Cu_2O are formed, while CuO and CeO_2 are formed coupled with calcinations. The SEM shows that the CuO/CeO_2 ribbons with a homogeneous pore/grain structure are thermally stable up to 600˚C because uniform CeO_2 particles are dispersedly loaded on the fine CuO grains of the porous structure, which is validated by TEM again. Meanwhile, the Raman spectra show that the concentration of oxygen vacancies reach a maximum value when the calcining temperature at 600˚C. In addition, the gas chromatograph results show that the dealloyed $Al_{78}Cu_{20}Ce_2$ ribbons with calcined at 600˚C have the best active catalysis for CO oxidation and the rates of CO conversation reaching at 50% and 100% are 150˚C and 320˚C, respectively, owing to the synergetic effects of the CuO and CeO_2 species.

Keywords

Dealloying, Nanoporous, CuO, CeO_2, CO Oxidation

1. Introduction

Cerium oxide is an important rare earth oxide and has been widely investigated in the automotive exhaust purification, oxygen storage and release catalysis, and solid oxide fuel cell applications [1]-[3]. For such applications, especially for automobile exhaust gas emission control, CeO_2 performs the following functions: 1) it stabilizes the catalyst against metal dispersion; 2) it stores and releases oxygen; and 3) it improves CO oxidation and NO_x reduction [4]. Meanwhile, copper is an attractive metal for industrial applications owing to its higher stability and lower cost, coupled with CuO with high catalytic activities toward CO and hydrocarbon oxidation, to which are paid much attention. In recent years, the Cu-Ce-O system has been found to be effective catalyst for low temperature CO oxidation and was widely studied with the hope that it could be used as a replacement for

*Corresponding author.

How to cite this paper: Wei, C.H., Zhang, X.L., Lu, F.F., Song, Y.Y. and Sun, Z.B. (2015) The Preparation and Catalytic Performance of Nanoporous CuO/CeO_2 Composites. *Journal of Materials Science and Chemical Engineering*, **3**, 154-161.
http://dx.doi.org/10.4236/msce.2015.37021

expensive precious metal catalysts.

What's more, it has been identified that the enhanced catalytic activities of CeO_2-CuO nanocomposites are attributed to their synergetic interface interaction [5] [6]. Generally, a CuO/CeO_2 catalyst is synthesized by impregnation and precipitation methods. Gregorio Marba'n *et al.* have reparted that the CuO_x/CeO_2 nanocatalysts are synthesized using the silica aquagel co-precipitation technique and tested for the preferential oxidation of CO [7]. In addition, Xiucheng Zheng *et al.* have reported that CuO/CeO_2 catalysts prepared thermal decomposition combined with impregnation can significantly promote the low-temperature CO oxidation, which were studied by using a microreactor-GC system. It suggests that the physical properties of CeO_2 supports affect the catalytic activity of the CuO/CeO_2 catalysts [4]. Besides, Weihua Shen *et al.* have reported that mesoporous cerium dioxide has been synthesized using the ordered mesoporous silica KIT-6 as hard template and a series of different amounts of CuO have been modified to this CeO_2 replica by wet impregnation [8]. It is easily observed that the above fabrication procedure are too complex to achieve large scale industrialization production, while the higher production cost and the environment unfriendly restrict its commercial application.

Even so, there are few results about nanoporous CuO/CeO_2 composites by dealloying. As far as I know, monolithic nanoporous CuO/CeO_2 composites prepared by dealloying coupled with calcination treatment have not been reported so far. In our present work, we take a more effective and controllable approach to prepare nanoporous metals, which is dealloying [9]. The objective is aimed at developing a high-performance catalyst and gain a better understanding of the interfacial interaction between transition metals and CeO_2 while studying their catalytic activity in low temperature CO oxidation. It is expected that the strategy reported here can not only be extended to other nanoporous metal-oxidate materials for widespread applications, but also offer a new direction for nanocomposites.

2. Experimental

2.1. Preparation of the Al-Cu-Ce Precursor Alloy

$Al_{80-x}Cu_{20}Ce_x$ (x = 0.5, 1, 2, 3, at%) alloy with nominal compositions were prepared from pure Al, Cu and Ce by arc-melting in a arc furnace at an argon atmosphere. Subsequently, the ingot was inserted into a quartz tube and heated by high frequency induction to the required temperature. Melt-spun $Al_{80-x}Cu_{20}Ce_x$ ribbons were obtained by a single roller melt spinning with a speed of 33 m/s. The thickness of the obtained ribbons was approximately30 μm, and the width about 3 mm.

2.2. Preparation of the Nanoporous CuO/CeO_2 Composite

The melt-spun ribbons were dealloyed in a 5 wt% NaOH aqueous solution at room temperature until no obvious bubbles emerged. The dealloyed ribbons were rinsed in distilled water several times and rinsed in anhydrous ethanol, and then dried at 50˚C in a drying oven box. At last, the dealloyed ribbons were calcined for 1 h in a muffle furnace at 300˚C, 450˚C, 600˚C, 800˚C and 1000˚C, respectively.

2.3. Characterization

The phase structures of the as-quenched $Al_{80-x}Cu_{20}Ce_x$ (x = 0.5, 1, 2, 3, at%) ribbons, and the as-dealloyed and as-calcinated samples were analyzed by a Bruker D8 advanced X-ray Diffraction (XRD). The microstructures were observed by a JSM-7000F Scanning Electron Microscope (SEM, JEOL Ltd) and a JEM-2100 High Resolution Transmission Electron Microscope (HRTEM, JEOL Ltd). The elemental distribution of the sample was analyzed by a JEM-2100F Transmission Electron Microscope equipped with an Energy Dispersive X-ray Spectroscopy (EDS, INCAX-Sight Oxford). The dealloyed and calcined $Al_{78}Cu_{20}Ce_2$ samples were investigated by a Laboratory Ram JY-HR800 (HORIBA Jobin Yvon, France) spectrometer at an output laser power of 17.0 mW. The exposure time was 2 s and the operating wavelength 632.8 nm.

2.4. The Characterization of CO Oxidation Performance

The activity of the catalyst (about 100 mg) was tested using a GC7900 gas chromatograph equipped with a thermal conductivity detector (FID). Meanwhile, the gases contained 1% CO and 99% O_2 balanced with nitrogen and the total gas flow rate were 0.01 mL/s.

3. Results and Discussion

3.1. Microstructures of the Nanoporous CuO/CeO_2 Composite

Figure 1 shows the XRD patterns of as-quenched, dealloyed and as-calcined (x = 0.5, 1, 2, 3, at%) samples. For the as-quenched $Al_{79.5}Cu_{20}Ce_{0.5}$ and $Al_{79}Cu_{20}Ce_1$ ribbons, as shown in **Figure 1(a)**, the peaks of α-Al and Al_2Cu appear. When Ce content was increased to 2 and 3 at%, the α-Al, Al_2Cu and Al_2Ce can be measured, meanwhile, the diffraction peaks of Al_2Cu disappear. It indicates that cerium mainly dissolves in aluminum solid solution when its content is very low, but a small amount of cerium compounds appear when the amount of cerium is more. After the $Al_{80-x}Cu_{20}Ce_x$ (x = 0.5, 1, 2, 3, at%) ribbons are dealloyed, as shown in **Figure 1(b)**, all the samples only consist of Cu and Cu_2O. **Figure 1(b)** reveal that the diffraction peaks are low and broad, indicating that constitution phases don't crystallize fully. The peaks corresponding to the Ce, as shown in **Figure 1(b)**, have not be detected, but the EDS analysis shows that the cerium in precursor alloys loss a little during dealloying. When the dealloyed $Al_{78}Cu_{20}Ce_2$ samples are calcined at 300˚C - 1000˚C, the Cu and Cu_2O are oxidized to CuO. While the CeO_2 can be measured after the samples are calcined above 600˚C, which can be seen from **Figure 1(d)**. These results confirm that the CuO/CeO_2 composite are achieved through chemical dealloying combined with subsequent calcination.

Figure 2 shows the SEM images of the dealloyed $Al_{78}Cu_{20}Ce_2$ ribbons. The surface of the samples illustrate an ultrafine porous structure, as shown in **Figure 2(a)**. The cross-section, as shown in **Figure 2(b)**, shows a uniform porous structure. Pore channels with an average size of about 10 nm run throughout the whole ribbons and the pore walls exhibit a flake-like shape while each flake is made up of many small particles.

Furthermore, from **Figure 3(c)**, it can be seen that the surface of the samples calcined at 300˚C, 450˚C, 600˚C and 800˚C exhibits a bicontinuous nanoporous structure. While the energy dispersive X-ray spectroscope (EDS)

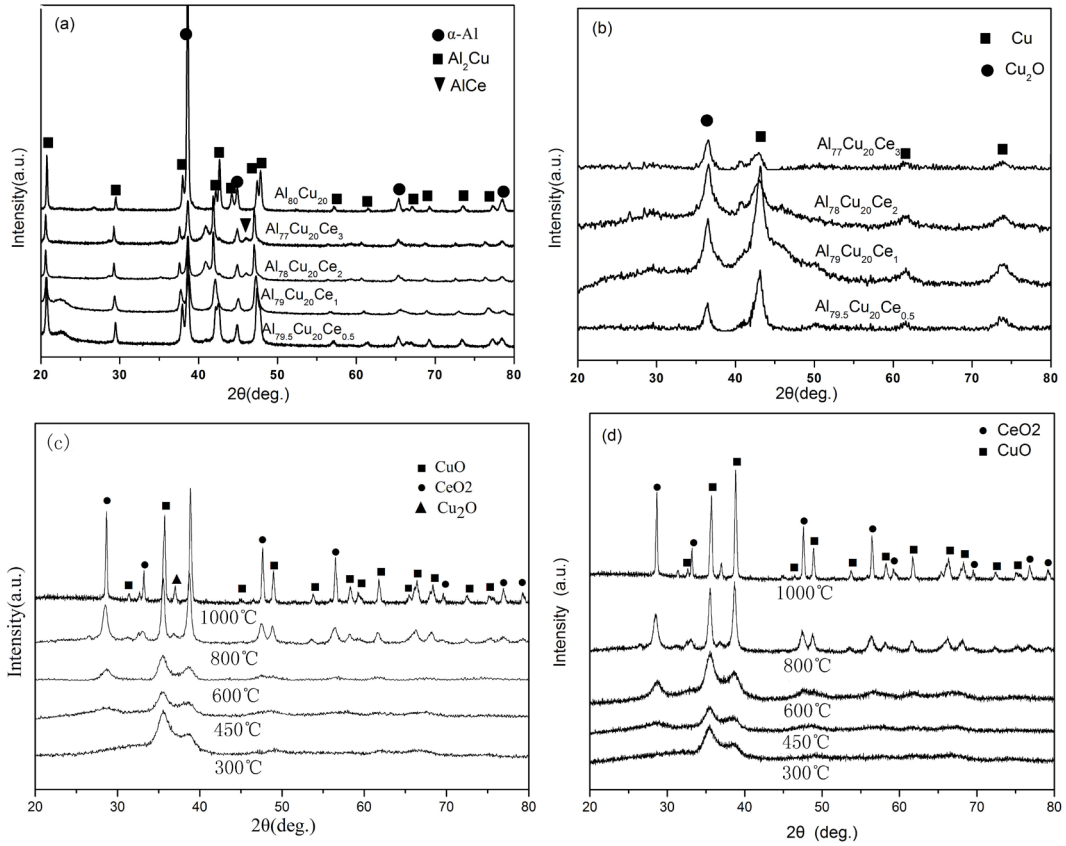

Figure 1. XRD patterns of the melt-spun $Al_{80-x}Cu_{20}Ce_x$(x = 0, 0.5, 1, 2, 3, at%) ribbons before and after dealloying in a 5 wt% NaOH solution (a); (b) and the dealloyed $Al_{80-x}Cu_{20}Ce_x$ (x = 0.5, 1, 2, 3, at%) samples calcined at 600˚C (c) and the dealloyed $Al_{78}Cu_{20}Ce_2$ sample calcined at 300˚C - 1000˚C (d).

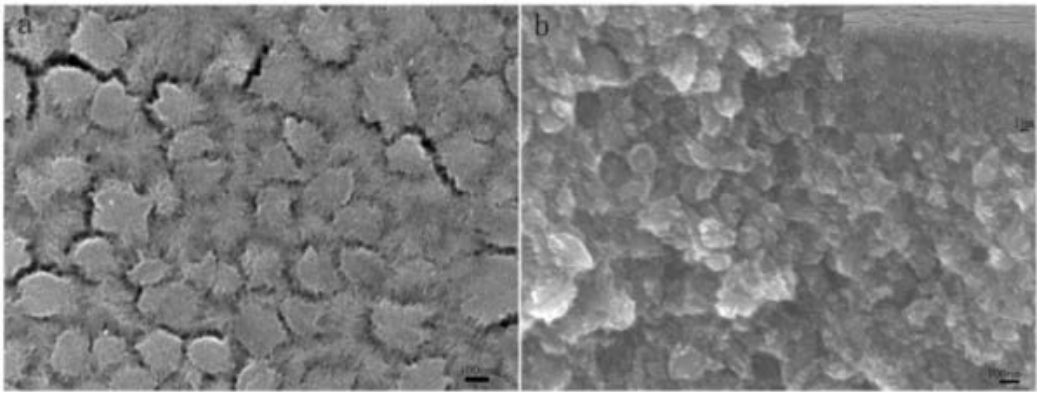

Figure 2. Plan-view and section-view SEM images showing the microstructures of the dealloyed $Al_{78}Cu_{20}Ce_2$ ribbons at room temperature (a) (b).

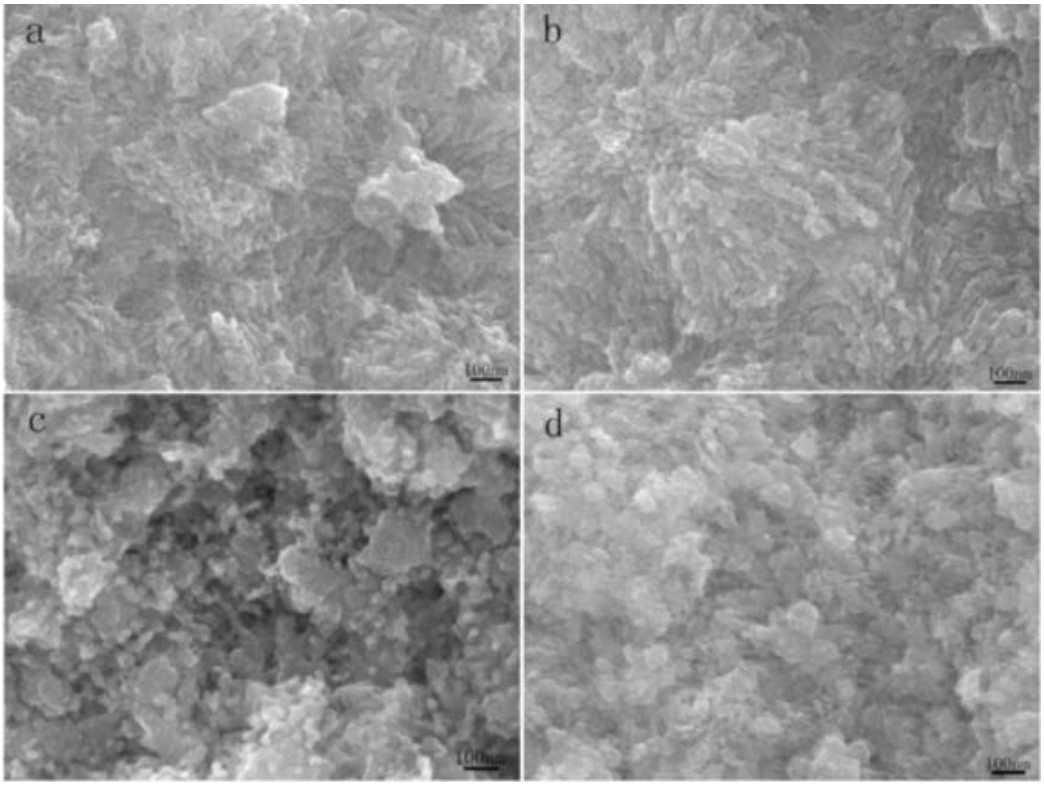

Figure 3. The cross-view SEM images showing the microstructures of the dealloyed $Al_{78}Cu_{20}Ce_2$ ribbons calcined at 300˚C (a); 450˚C (b); 600˚C (c) and 800˚C (d).

analysis demonstrates that the nanoporous samples are composed of Cu, Ce, and the residual Al. The Cu:Ce atom ratio is 87:7, which indicates that only a small amount of Ce atoms in the $Al_{78}Cu_{20}Ce_2$ alloy has been lost during dealloying as shown in **Table 1**. With calcination temperature increasing, it can be clearly observed obvious grain coarsening and higher pore size from the cross-section review (**Figures 3(a)-(c)**). While the sample calcined at 600˚C, some big pore can be observed, as shown in **Figure 3(c)**. When the sample calcined at 800˚C, the pore walls transform from flake-like shape into block-like shape, and the porosity significantly decreases, coupled with the nanoporous structure has collapsed. The results show that the nanoporous structure will be coarsening in the calcination process owing to grain recrystallization and agglomeration. Besides, CeO_2 is the most commonly additives using for CO catalytic oxidation, which can reduce the agglomeration of active component and improve the stability of it by interacting with active component [10].

TEM and HRTEM images of the dealloyed $Al_{78}Cu_{20}Ce_2$ sample calcined at 600˚C are displayed in **Figure 4**. **Figure 4(a)** shows that the sizes of the pore channels and grains are in agreement with the SEM observation. It can be seen that many nanoparticles are loaded on the surface of the CuO grains, which are CeO_2.The formation mechanism of the nanoporous Cu prepared by the dealloying of melt-spun Al-Cu alloys in acidic or alkaline aqueous solution has been extensively studied. The dealloying process is essentially the selective dissolution of Al atoms from the precursor alloys and the rearrangement of Cu atoms, resulting in the formation of the nanoporous Cu with a three-dimensional porous structure. In this report, the as-quenched $Al_{78}Cu_{20}Ce_2$ alloy contains a-Al, Al_2Cu and Al_2Ce (**Figure 1(a)**). It is known that Al is easy to react with NaOH aqueous solution to produce soluble $NaAlO_2$ but Ce cannot react with NaOH aqueous solution. As the a-Al and Al_2Ce compound are decomposed, the released Cu atoms and Ce atoms diffuse, rearrange and accumulate, resulting in the formation of a nanoporous structure. When the samples are calcined at specific temperature, the released Ce atoms from the decomposed Al_2Ce remain in the porous structure, and react with oxygen to form CeO_2 in situ while Cu is oxidized to CuO. While the Cu and Ce atom will interact with oxygen in air forming CeO_2 and CuO. Accordingly, CeO_2 is deposited on the surface of the CuO grains, which produce many interface between CeO_2 and CuO (**Figure 4(b)**). It demonstrates that we have successfully prepared nanoporous CuO/CeO_2 composite.

Figure 5(a) shows the Raman spectra of the dealloyed $Al_{80-x}Cu_{20}Ce_x$ (x = 0.5, 1, 2, 3, at%) ribbons calcined at 600˚C. It can be observed that the sample $Al_{79.5}Cu_{20}Ce_{0.5}$ shows three prominent peaks at about 292, 340 and 589 cm^{-1}. The peak at 292 and 340 cm^{-1} represent CuO while the peak at 589 cm^{-1} represent CeO_2,which is attributed to oxygen vacancies generated as charge compensation for the defects induced by the incorporation of ceria cations into the copper lattice [11] [12]. Most importantly, the peak at 589 cm^{-1} is much broad, which illustrates that CeO_2 hasn't crystallized or crystallized inadequately. Along with the content of cerium increasing, the peak at 461 cm^{-1} appears, which represent the F_{2g} of CeO_2 [13], deriving from the dealloyed $Al_{80-x}Cu_{20}Ce_x$ (x = 1, 2) ribbons calcined at 600˚C, whose intensity gradually get stronger. The results indicate that the nanoporous CuO/CeO_2 composite is formed while crystallinity increases and grain grow, which is consistent with the XRD results (**Figure 1(c)**). However, the peaks at 461 and 589 cm^{-1} turn to be weak accompanied with the peaks at 292 and 340 cm^{-1} becoming much weak when the content of cerium reaching at 3%, which well demonstrates that the perfect content of cerium is 2%.

In the calcining process of porous Cu (Ce) alloy, the Cu and Ce are oxidized into CuO and CeO_2 respectively

Table 1. EDS results of the nanoporous Cu prepared by chemical dealloying of the $Al_{80-x}Cu_{20}Ce_x$ (x = 0.5, 1, 2, 3, at%) alloy at room temperature for different time.

Samples	Al (at%)	Cu (at%)	Ce (at%)
$Al_{79.5}Cu_{20}Ce_{0.5}$	7.13	90.48	2.39
$Al_{79}Cu_{20}Ce_1$	6.48	88.39	5.13
$Al_{78}Cu_{20}Ce_2$	5.69	87.09	7.22
$Al_{77}Cu_{20}Ce_3$	7.15	80.42	12.43

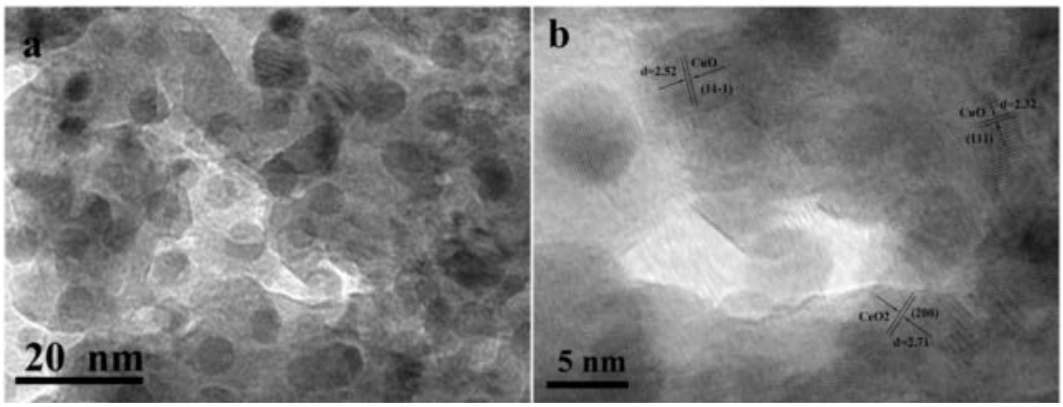

Figure 4. TEM and HRTEM images of the dealloyed $Al_{78}Cu_{20}Ce_2$ sample calcined at 600˚C (a); (b).

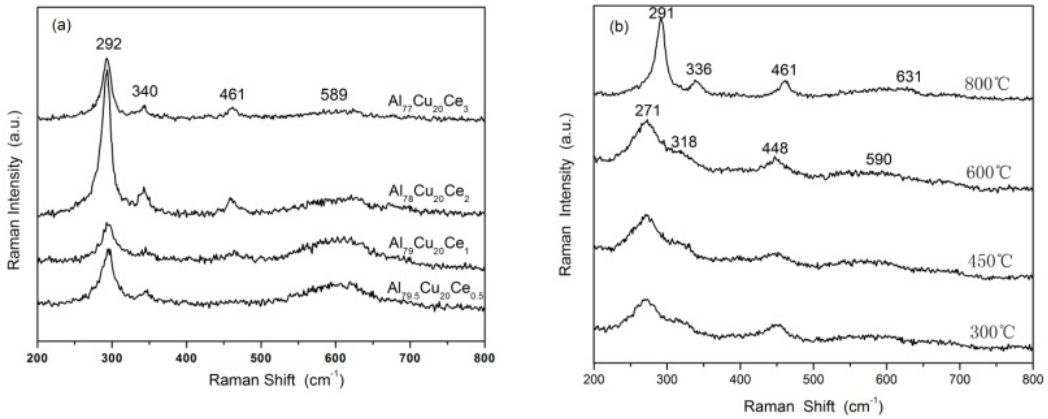

Figure 5. Raman spectra of the dealloyed $Al_{80-x}Cu_{20}Ce_x$(x = 0.5, 1, 2, 3, at%) ribbons calcined at 600˚C, respectively (a) and the dealloyed $Al_{78}Cu_{20}Ce_2$ sample calcined at 300˚C - 800˚C (b).

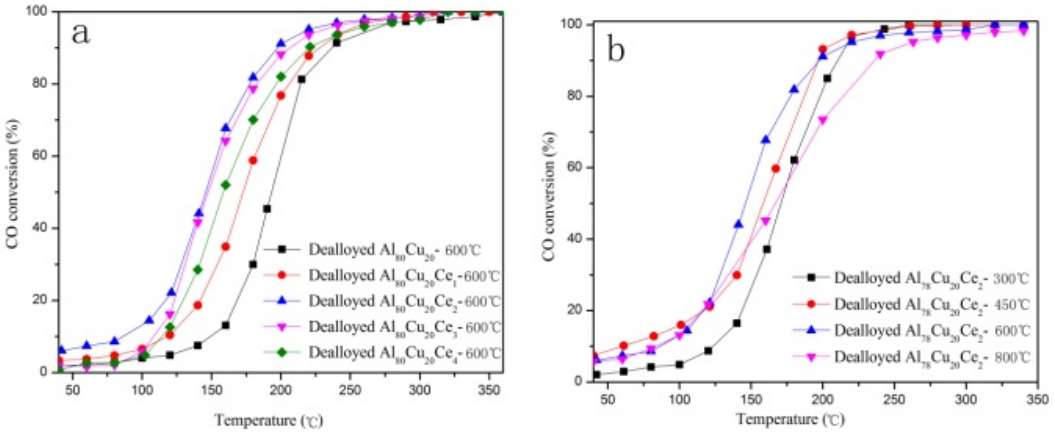

Figure 6. Catalytic activity of the dealloyed $Al_{80}Cu_{20}$ and $Al_{80-x}Cu_{20}Ce_x$ (x = 0.5, 1, 2, 3, at%) samples calcined at 600˚C (a); Catalytic activity of the dealloyed $Al_{78}Cu_{20}Ce_2$ sample calcined at 300˚C - 800˚C (b).

under the condition of rich oxygen, while Ce^{4+} enter into CuO lattice and then form $Ce_{1-x}Cu_xO_{2-\delta}$ solid solution. These particles distribute on the surface of porous CuO, which makes CeO_2 load on nanoporous CuO in situ. Besides, Cu^{2+} enter into CeO_2 lattice and then form doped defect, resulting in the formation of a large number of oxygen vacancies in the bulk due to the different valence state of Cu^{2+} and Ce^{4+} and the precipitation of lattice oxygen. In addition, the concentration of oxygen vacancy is highly affected by the Ce content and calcination temperature.

3.2. Catalytic Activity for CO Oxidation

Figure 6(a) shows the conversion rate of CO catalytic oxidation of the dealloyed $Al_{80}Cu_{20}$ and $Al_{80-x}Cu_{20}Ce_x$ (x = 1, 2, 3, 4 at%) samples calcined at 600˚C. Obviously, the catalytic activity of the pure nanoporous CuO is lower than the CuO/CeO_2 composites, and the CO conversion rates reaching at 50%, and 100% are taken place in 180˚C, and 350˚C respectively. There is a large difference in the temperatures of 50% conversion of the $Al_{80-x}Cu_{20}Ce_x$ (x = 1, 2, 3, 4 at%) samples, which is lower than 180˚C. Meanwhile, the temperatures of 50% conversion of the $Al_{78}Cu_{20}Ce_2$ is the lowest (≈130˚C). It can be easily seen that catalytic activity of the nanoporous CuO improves with the addition of Ce, which differs with different Ce content. The combined results of the HRTEM, XRD and Raman analyses show that the various CuO supports had different surface defects that led to the loading differences of CeO_2 which entered into the copper lattice or dispersed on the copper surface. Luo *et al.* [14] also suggested that the dispersed CuO was responsible for the low-temperature CO oxidation in CuO/CeO_2 catalysts. The results indicated that CeO_2 supports affect the synergistic effect, subsequently affect

the catalytic activity of the corresponding CuO/CeO_2 catalysts.

Catalytic activity of the dealloyed $Al_{78}Cu_{20}Ce_2$ sample calcined at 300˚C - 800˚C are presented in **Figure 6(b)**. The catalysts calcined at 600˚Cexhibited the best catalytic activity in comparision with the samples calcined at 300˚C, 450˚C, 800˚C, respectively, which reaches 50% conversion at 150˚C and reaches 50% conversion at 320˚C. Obviously, the conversion rate of CO are highly affected by the calcination temperature. Catalytic activity of the dealloyed $Al_{78}Cu_{20}Ce_2$ sample increase firstly and then decrease with the calcination temperature increasing, which is attributed to the reduction of oxygen vacancy. In addition, the concentration of oxygen vacancy of catalysts are the highest when it calcined at 600˚C,with the increase of calcination temperature, the initial conversion rate of CO rise from 3% to 8%. When the reaction temperature increased further, the conversion rate of CO continue to increase.

4. Conclusion

We have successfully developed a novel approach to prepare CuO/CeO_2 catalyst by a simple dealloying of melt-spun $Al_{80-x}Cu_{20}Ce_x$ (x = 0.5, 1, 2, 3, at%) ribbons in a 5 wt% NaOH aqueous solution, followed by calcining at different temperatures. A larger number of oxygen vacancies are formed in the CeO_2 nanoparticles loaded on the CuO grains with an increase of the calcination temperature. Therefore, the nanoporous CuO/CeO_2 composite exhibits enhanced activities for CO oxidation due to the enhancement of interfacial interactions between CuO and CeO_2.

Acknowledgements

The authors gratefully acknowledge financially supported from the National Natural Science Foundation of China (Grant No. 51371135)

References

[1] Li, G.J., Lu, F.F., Wei, X., Song, X.P., Sun, Z.B., *et al.* (2013) Nanoporous Ag-CeO_2 Ribbons Prepared by Chemical Dealloying and Their Electrocatalytic Properties. *Journal of Materials Chemistry A*, **1**, 4974-4981. http://dx.doi.org/10.1039/c3ta01506h

[2] Moreno, M., Bergamini, L., Baronetti, G.T., Laborde, M.A. and Mariño, F.J. (2010) Mechanism of CO Oxidation over CuO/CeO_2 Catalysts. *International Journal of Hydrogen Energy*, **35**, 5918-5924. http://dx.doi.org/10.1016/j.ijhydene.2009.12.107

[3] Gu, X.R., Li, H., Liu, L.C., Tang, C.J., Gao, F. and Dong, L. (2014) Promotional Effect of CO Pretreatment on CuO/CeO_2 Catalyst for Catalytic Reduction of NO by CO. *Journal of Rare Earth*, **32**, 139. http://dx.doi.org/10.1016/S1002-0721(14)60043-0

[4] Zheng, X.C., Zhang, X.L., Wang, X.Y., Wang, S.R. and Wu, S.H. (2005) Preparation and Characterization of CuO/CeO_2 Catalysts and Their Applications in Low-Temperature CO Oxidation. *Applied Catalysis A*: *General*, **295**, 142-149. http://dx.doi.org/10.1016/j.apcata.2005.07.048

[5] Kim, D.H. and Cha, J.E. (2003) A CuO-CeO_2 Mixed-Oxide Catalyst for CO Clean-Up by Selective Oxidation in Hydrogen-Rich Mixtures. *Catalysis Letters*, **86**, 107-112. http://dx.doi.org/10.1023/A:1022671327794

[6] Bruix, A., Rodriguez, J.A., Ram'ırez, P.J., Senanayake, S.D., Evans, J., Park, J.B., Stacchiola, D., Liu, P., Hrbek, J. and Illas, F. (2012) A New Type of Strong Metal-Support Interaction and the Production of H_2 through the Transformation of Water on $Pt/CeO_{(X)}/TiO_2$ (110) Catalysts. *Journal of the American Chemical Society*, **134**, 8968-8974. http://dx.doi.org/10.1021/ja302070k

[7] Marbán, G., López, I. and Valdés-Solís, T. (2009) Preferential Oxidation of CO by CuO_X/CeO_2 Nanocatalysts Prepared by SACOP. Mechanisms of Deactivation under the Reactant. *Applied Catalysis A*: *General*, **361**, 160-169. http://dx.doi.org/10.1016/j.apcata.2009.04.014

[8] Shen, W.H., Dong, X.P., Zhu, Y.F., Chen, H.R. and Shi, J.L. (2005) Mesoporous CeO_2 and CuO-Loaded Mesoporous CeO_2: Synthesis, Characterization, and CO Catalytic Oxidation Property. *Microporous and Mesoporous Materials*, **85**, 157-162. http://dx.doi.org/10.1016/j.micromeso.2005.06.006

[9] Wang, Z.F., Wang, L.J., Qin, C.L., Liu, J.Y., Li, Y.Y. and Zhao, W.M. (2014) Tailored Dealloying Products of Cu-Based Metallic Glasses in Hydrochloric Acid Solutions. *Materials Research*, **17**, 1003-1009. http://dx.doi.org/10.1590/S1516-14392014005000089

[10] Jia, A.-P., Jiang, S.-Y., Lu, J.-Q., and Luo, M.-F. (2010) Study of Catalytic Activity at the CuO-CeO_2 Interface for CO Oxidation. *The Journal of Physical Chemistry C*, **114**, 21605-21610. http://dx.doi.org/10.1021/jp108556u

[11] Chen, G.X., Li, Q.L., Wei, Y.C., Fang, W.P. and Yang, Y.Q. (2013) Low Temperature CO Oxidation on Ni-Promoted CuO-CeO_2 Catalysts. *Chinese Journal of Catalysis*, **34**, 322-329. http://dx.doi.org/10.1016/S1872-2067(11)60468-3

[12] Spanier, J.E., Robinson, R.D., Zhang, F., Chan, S.-W. and Herman, I.P. (2001) Size-Dependent Properties of CeO_{2-y} Nanoparticles as Studied by Raman Scattering. *Physical Review B*, **64**, 245407-245414. http://dx.doi.org/10.1103/PhysRevB.64.245407

[13] López Cámara, A., Cortés Corberán, V., Barrio, L., Zhou, G., Si, R. and Hanson, J.C. (2014) Improving the CO-PROX Performance of Inverse CeO_2/CuO Catalysts: Doping of the CuO Component with Zn. *The Journal of Physical Chemistry C*, **118**, 9030-9041. http://dx.doi.org/10.1021/jp5009384

[14] Luo, M.-F., Zhong, Y.-J., Yuan, X.-X. and Zheng, X.-M. (1997) TPR and TPD Studies of CuO/CeO_2 for Low Temperature CO Oxidation. *Applied Catalysis A*: *General*, **162**, 121-131. http://dx.doi.org/10.1016/S0926-860X(97)00089-6